Collective Intermolecular Motions Dominate the Picosecond Dynamics of Short Polymer Chains

Humphrey Morhenn*
Forschungs-Neutronenquelle Heinz Maier-Leibnitz (FRM II) and Lehrstuhl für Funktionelle Materialien, Physik-Department, Technische Universität München, 85747 Garching, Germany and Friedrich-Alexander-Universität Erlangen-Nürnberg, Lehrstuhl für Kristallographie und Strukturphysik, Staudtstrasse 3, 91058 Erlangen, Germany

Sebastian Busch
Department of Biochemistry, University of Oxford, South Parks Road, OX1 3QU Oxford, United Kingdom

Hendrik Meyer
Institut Charles Sadron, Université de Strasbourg, CNRS UPR22, 67034 Strasbourg, France

Dieter Richter
Institut für Festkörperforschung, Forschungszentrum Jülich GmbH, 52425 Jülich, Germany

Winfried Petry
Forschungs-Neutronenquelle Heinz Maier-Leibnitz (FRM II) and Lehrstuhl für Funktionelle Materialien, Physik-Department, Technische Universität München, 85747 Garching, Germany

Tobias Unruh†
Friedrich-Alexander-Universität Erlangen-Nürnberg, Lehrstuhl für Kristallographie und Strukturphysik, Staudtstrasse 3, 91058 Erlangen, Germany

(Received 7 February 2013; published 22 October 2013)

Neutron scattering and extensive molecular dynamics simulations of an all atom $C_{100}H_{202}$ system were performed to address the short-time dynamics leading to center-of-mass self-diffusion. The simulated dynamics are in excellent agreement with resolution resolved time-of-flight quasielastic neutron scattering. The anomalous subdiffusive center-of-mass motion could be modeled by explicitly accounting for viscoelastic hydrodynamic interactions. A model-free analysis of the local reorientations of the molecular backbone revealed three relaxation processes: While two relaxations characterize local bond rotation and global molecular reorientation, the third component on intermediate times could be attributed to transient flowlike motions of atoms on different molecules. The existence of these collective motions, which are clearly visualized in this Letter, strongly contribute to the chain relaxations in molecular liquids.

DOI: 10.1103/PhysRevLett.111.173003 PACS numbers: 33.15.Vb, 61.25.Em, 66.10.C−

The dynamics of molecular liquids cover a broad range of time scales, ranging from the fast local relaxation of the atomic bonds to global motions of the whole chain. The dynamics occurring on time scales in between are more complex due to the interplay of intra- and intermolecular interactions. For short chains, long enough to show Gaussian chain statistics, the Rouse theory was developed to describe the chain dynamics [1]. However, neutron scattering experiments and molecular dynamics (MD) simulations on a polyethylene melt of $C_{100}H_{202}$, which should be an ideal Rouse chain [2], showed that the Rouse model is only able to describe the dynamics on a length scale of the whole molecules but fails to predict rather local relaxations [3]. Another MD simulation study on this system unveiled a distinct dynamical process on intermediate time scales (between the time scales of dihedral rotation and molecular reorientation) when relaxations on a longer length scale were analyzed [4]. Similar results were found for polyisobutylene, *cis*-1,4-polybutadiene, polypropylene, and polyethylene terephthalate [5]. There is no true understanding of the nature of this process to date; it is only known that a change in pressure has an effect on this intermediate relaxation [6]. In this Letter we present a combined neutron scattering and MD simulation study which unveils that on intermediate times the dynamics of the monomers are dominated by intermolecular collective motions. These transient flowlike motions coincide with a subdiffusive behavior of the center-of-mass (c.m.) diffusion, which represents a failure of the assumption of white noise in the classical Rouse model. This is the first experimentally validated simulation supporting the recent theory presented by Farago *et al.*, who have accounted for viscoelastic hydrodynamic interactions and state that hydrodynamic effects lead to anomalous center-of-mass diffusion in polymer melts [7].

For these studies resolution resolved quasielastic neutron scattering experiments were conducted at the

cold neutron time-of-flight spectrometer TOFTOF at the Forschungs-Neutronenquelle Heinz Maier-Leibnitz (FRM II) [8]. By tuning the instrumental resolution from 23 μeV to 3 meV (FWHM), the corresponding observation time was varied on a time scale from 118 to 1.1 ps. The instrument settings are given elsewhere [9]. The $C_{100}H_{202}$ sample (melting temperature $T_m \approx 388.4$ K [10]) was measured at $T = 509$ K using a thin-walled aluminum hollow cylinder as the sample holder with a sample layer thickness of 0.1 mm [11]. The collected data were corrected for detector efficiency, self-absorption effects, background scattering of the aluminum sample holder, and were normalized to a vanadium standard. The resulting spectra were rebinned to spectra of constant scattering vector Q, and a numerical Fourier transform was performed to obtain the intermediate scattering function $I(Q, t)$ [9]. The sample $I(Q, t)$ with different observation times were divided by the corresponding $I(Q, t)$ of vanadium and then straightforward merged, as described previously [9], resulting in a single master curve. Because of the perfect overlap of the spectra (see Fig. 1), one can easily cover 3 orders of magnitude in time at TOFTOF.

Molecular dynamics simulations were performed using the program package GROMACS 4.5 [12], with the OPLS-AA force field and optimized parameters [13]. In order to lower the melting temperature, which is known to be too high using this force field [14], the explicit 1–4 pair interactions were neglected. This does not have a major influence on the dynamics, as already demonstrated for a short chain $C_{16}H_{34}$ system [9]. The Nosé-Hoover thermostat and Parinello-Rahman barostat were applied to simulate a NPT ensemble. The simulation parameters are as described previously in Ref. [9]. The simulation system, containing 4096 $C_{100}H_{202}$ molecules, was equilibrated for more than 10 ns before production runs were performed for up to 20 ns at $T = 509$ K. This system is significantly larger than the $C_{100}H_{202}$ melt simulated in Ref. [3], which makes it possible for hydrodynamic interactions to fully develop. Running on a supercomputer with 512 processors resulted in 1.5 ns/day computation speed. For validation, the coherent and incoherent intermediate scattering functions $I(Q, t)$ were calculated using the program NMOLDYN [15], weighted corresponding to the respective scattering cross sections and summed up to result in the total $I(Q, t)$.

The simulated and measured intermediate scattering functions match over the entire Q and t scale studied, as exemplarily shown in Fig. 1. According to this outstanding agreement of the experimental data and simulated trajectories, it can be assumed that the simulated dynamics represent the measured ones.

Large scale dynamics of the MD simulations were analyzed by calculating the mean-square displacements (MSD) of the c.m. coordinates of the molecules (see Fig. 2). The self-diffusion coefficient determined by a

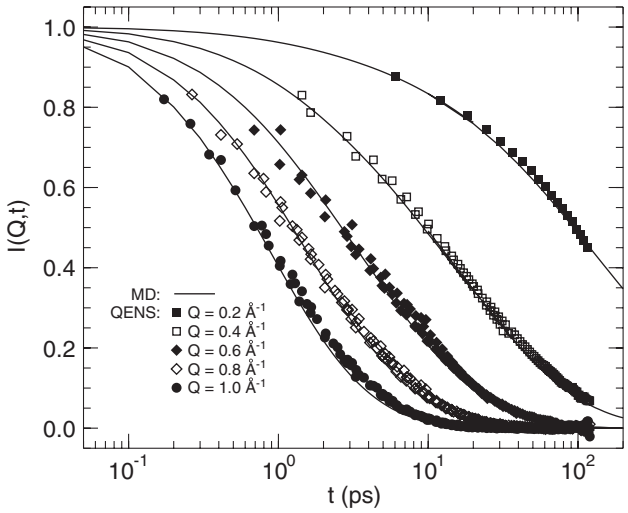

FIG. 1. Normalized intermediate scattering functions as measured with quasielastic neutron scattering (QENS, symbols) and calculated from the molecular dynamics simulation (MD, solid lines) for different values of momentum transfer Q at $T = 509$ K. The merged QENS spectra are divided by constant factors (ranging from 1.10 to 1.35) for scaling, as $I(Q, t = 0)$ is not well defined in the experiment due to the limited kinematic range of the neutrons. The QENS and MD simulation data are in very good agreement.

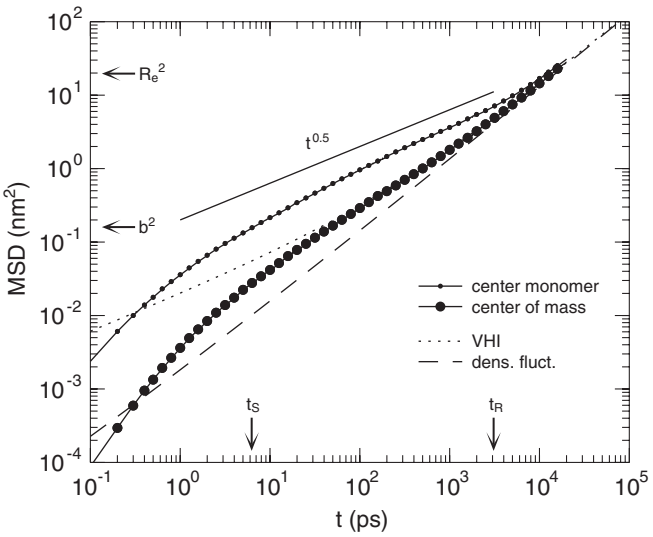

FIG. 2. Mean-square displacement (MSD) obtained from the simulation at $T = 509$ K for the center monomers of the $C_{100}H_{202}$ chains (small symbols) and for the center-of-mass coordinates (c.m., big symbols). Additionally plotted are theoretical predictions considering viscoelastic hydrodynamic interactions (dotted line, Eq. (34) in [19]) and density fluctuations (dashed line, Eq. (30) in [18]) to account for the subdiffusive behavior of the c.m. MSD. The arrows indicate the mean-square chain end-to-end distance R_e^2, the squared statistical segment length b^2, and the segmental t_S and Rouse t_R relaxation time, to visualize the range of validity of the models. The relaxation times were extracted from a standard Rouse analysis of the normal modes [17]. The solid line represents a $t^{1/2}$ power law.

linear fit (not shown) yields $D_{\text{c.m.}}^{\text{MSD}} = 2.38 \times 10^{-6}$ cm^2/s, which is in fair agreement with an extrapolation of pulsed-field gradient nuclear magnetic resonance data from Pearson *et al.* [16] as well as with the values reported in Ref. [3].

A clear subdiffusive behavior of the c.m. MSD can be identified throughout the whole picosecond range, contrary to the Rouse theory which predicts a linear dependence for all times [17]. Two alternative approaches have been proposed by Farago *et al.* to model the subdiffusive scaling, accounting for density fluctuations [18] and viscoelastic hydrodynamic interactions (VHI) [19]. The c.m. MSD predicted by both theories is plotted in Fig. 2. While the effect of density fluctuations is too weak to describe the subdiffusive behavior, the theory of VHI-controlled chain dynamics represents the observations well. The corresponding expression for the c.m. MSD derived from the VHI theory is [19]

$$\text{MSD}_{\text{c.m.}}^{\text{VHI}} \simeq b^2\left[\frac{\pi}{2}\frac{Wt}{N} + \frac{96}{(3\pi)^{3/2}}\frac{1}{nb^3}\left(\frac{Wt}{N}\right)^{1/2}\right], \quad (1)$$

with the statistical segment length b, the number of monomers N, the monomer number density n, and a time constant W. In accordance with other studies [3,20] the parameters $b = 0.4$ nm and $n = 31$ nm^{-3} were used, while $W = 0.5$ ps^{-1} was determined postulating that the MSD of the center monomer is $b^2\sqrt{Wt}/6$ in the subdiffusive regime [18]. The first term in Eq. (1) represents the linear scaling as predicted by the Rouse theory, which describes the Fickean diffusion taking place at times longer than the Rouse time t_{R}. The second term accounts for the effect of VHIs, which dominates the c.m. MSD at times $t_{\text{S}} \ll t \ll t_{\text{R}}$. The great accordance proves that the VHI theory, which was developed to describe the motions of very long, unentangled, and flexible molecules, is also valid to model the global c.m. motion of the $C_{100}H_{202}$ chains.

Up to 100 ps there is only little motion of the whole molecules, the displacement of the c.m. coordinates is on the order of a few angstrom. The observable dynamics on this time scale is mainly due to the motions of single monomers, which show a more pronounced MSD. Since the displacements of the atoms cause local changes of the conformation of the molecules, eventually leading to translational motion on longer time scales, these local reorientations of the molecular backbone will be analyzed in the following.

Local chain dynamics were studied by calculating vector orientation autocorrelation functions (OACF)

$$P_i(t) = \langle \vec{e}_i(t)\vec{e}_i(0)\rangle. \quad (2)$$

The unit vector $\vec{e}$ is pointing in the direction of a single carbon–carbon bond, for different positions i of the bond along the molecular backbone. The resulting curves show a multistep decay (see Fig. 3). To describe the relaxations in a model-independent way, the CONTIN algorithm [21] was applied to fit a continuous distribution of exponential processes to the spectra according to

$$C(t) = \int_0^\infty F[\ln(\tau)]\exp^{-t/\tau}\mathrm{d}\ln(\tau). \quad (3)$$

Each exponential process is characterized by a characteristic relaxation time τ, and $F[\ln(\tau)]$ is the distribution of the relaxation times (DRT). The resulting DRT provides information about the number and dispersion of relaxation processes, as exemplarily illustrated in Fig. 3. This procedure was applied to the OACF of all carbon–carbon bonds along the molecular backbone separately. Figure 4 shows all resulting DRTs in a color plot. Three relaxation dispersions can clearly be identified and will be discussed in the following:

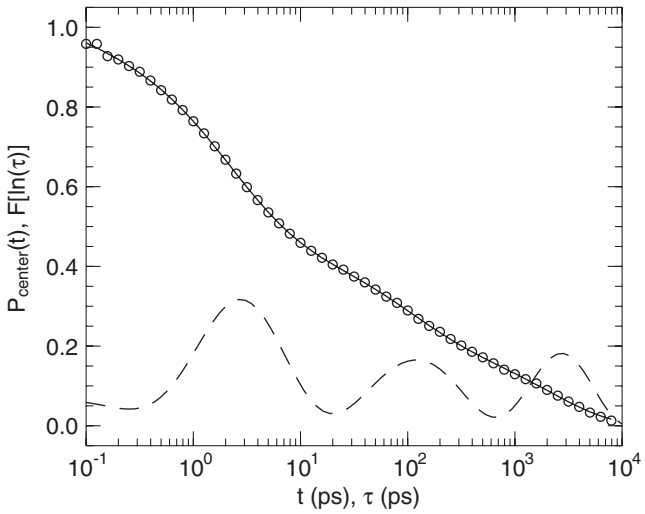

FIG. 3. Orientation autocorrelation function of the carbon–carbon bonds at a central position of the molecule (symbols), together with a fit of Eq. (3) (solid line). The resulting distribution of relaxation times (DRT, dashed line, multiplied by 10 for better visualization) shows three distinct relaxation processes.

The first peak is located at 2.6 ps and corresponds to the fast rotations of the dihedrals. This happens more frequently at the end of the molecule, due to the locally increased degrees of freedom [9].

An intermediate peak can be identified on a time scale of about 50–300 ps at rather central positions of the molecule. This time scale coincides with the subdiffusive regime of the MSD. Closer to the end of the chain this intermediate relaxation seems to overlay with the slowest relaxation peak.

The slowest relaxation process can be explained in terms of a rotational motion of the entire molecule. At the center of the chain this process shows a characteristic relaxation time of approximately 2.8 ns. This value is in good agreement with the value extracted from an exponential fit to the end-to-end vector OACF (2.9 ns, not shown). The bonds closer to the ends of the chain can reorient faster, because of the flexibility of the molecule.

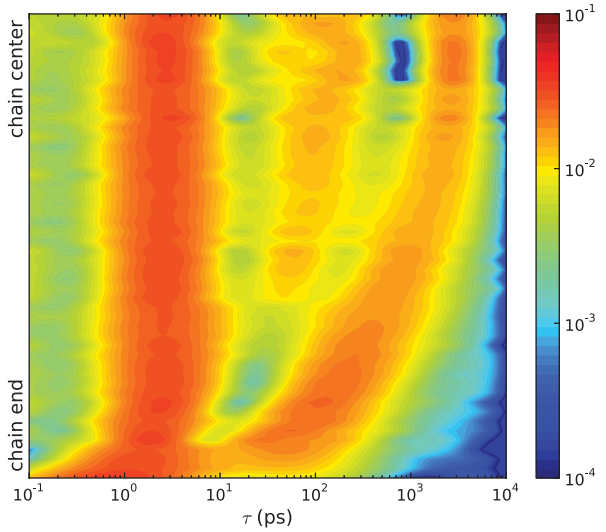

FIG. 4 (color). DRTs for different positions of the carbon–carbon bonds along the molecule (chain end to chain center). The amplitude of the DRTs is presented in color code. Three distinct chain relaxation processes can be identified at central positions of the molecular backbone.

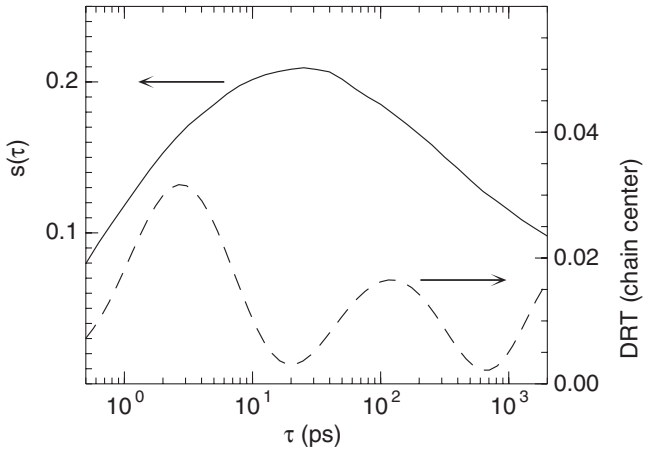

FIG. 5. Scalar product of unit displacement vectors of intermolecular neighboring carbon atoms $s(\tau)$ (solid line) and the DRT for the carbon–carbon bond reorientation at a central position of the $C_{100}H_{202}$ chain (dashed line). The maximum of $s(\tau)$ corresponds to the onset of the second relaxation process of the carbon–carbon bond vectors.

The origin of the intermediate relaxation was identified by evaluating correlated intermolecular dynamics: Let $\vec{r}_j(t)$ be the position vector of a carbon atom j at time t, setting up displacement vectors $\vec{u}_{j,t}(\tau) = \vec{r}_j(t+\tau) - \vec{r}_j(t)$. To measure the extent to which intermolecular neighboring atoms move collectively, the scalar product

$$s(\tau) = \left\langle \frac{\vec{u}_{j,t}(\tau)\vec{u}_{j',t}(\tau)}{|\vec{u}_{j,t}(\tau)||\vec{u}_{j',t}(\tau)|} \right\rangle_{j,t} \tag{4}$$

was calculated, with atom j' being the closest intermolecular carbon atom to atom j at time t. If the orientations of the atomic displacements were uncorrelated, the averaged scalar product would yield zero. A directed, collective motion results in $s(\tau) > 0$. The resulting spectrum is plotted in Fig. 5, together with the DRT of the carbon–carbon bond reorientation at a central position of the chain. Initially, at short times $\tau \ll 1$ ps, the atoms move uncorrelated. With increasing time, a correlation of the displacements develops: The intermolecular neighbors move preferably into the same direction. This collective behavior reaches its maximum at $\tau_{\max} \approx 25$ ps. Extending Eq. (4) by allowing j' to be any atom within a sphere of radius R around atom j at time t and averaging $s(\tau)$ for all these atoms will give similar curves $f(\tau, R) = \langle s(\tau)\rangle_{j'}$ again with a maximum at $\tau_{\max} \approx 25$ ps, which is fairly independent of R for $R < 2$ nm. The collectivity can be pictured as a flowlike motion of several atoms, which is also visible in 2D cuts of the molecular melt (see Fig. 6).

We speculate that the time $\tau_{\max}$ of maximum correlations of the intermolecular dynamics can be directly linked to the onset of the intermediate relaxation process. At $\tau_{\max}$ many atoms in large clusters move collectively into similar directions. The decorrelation of this flowlike behavior at $\tau > \tau_{\max}$ results in a relaxation of the local bond vectors, which causes an increase of the DRT. The fading of the intermolecular flow effect occurs on a wide time scale, which is reflected in the broad distribution of the intermediate relaxation process.

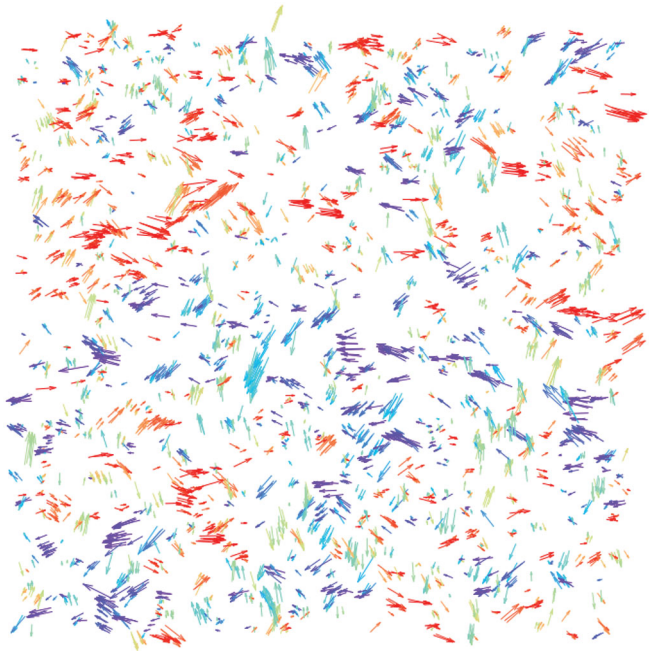

FIG. 6 (color). Displacement vectors of atoms during a time span of $\tau = 20$ ps in a 0.25 nm thick 2D cut (23.5×23.5 nm^2) of the simulation system. The colors highlight the direction of the displacements. Regions of correlated dynamics can easily be identified.

Summarizing, the chain dynamics of the $C_{100}H_{202}$ molecules at $T = 509$ K can be pictured as follows: At short times of some picoseconds the rotation of the dihedrals gives rise to the first relaxation of the carbon–carbon bond orientation, and the atoms displace 2–3 Å. Afterwards, the atoms start to see their surrounding, which leads to a transient collective flow of atoms in large clusters. The breakdown of these correlated motions corresponds to the second relaxation process. A third, even slower relaxation process is the rotation of the entire molecule, which occurs in the nanosecond time scale. On even longer times the displacement of the atoms is driven by the center-of-mass self-diffusion of the molecules.

This shows that the atomic motions in a molecular melt of short polymer chains show pronounced collective features on time scales framed by local and global chain relaxations. This transient flowlike behavior is driven by intermolecular interactions rather than by friction alone, as the Rouse model assumes, and contributes considerably to the local conformational changes of the molecular backbone. On an extended length scale the molecular center-of-mass MSD can be quantitatively reproduced using a model recently proposed and based on VHI [19]. Although collective intermolecular dynamics could clearly be identified and visualized, their impact on the observed intermediate relaxation process in terms of intramolecular contributions due to, e.g., chain stiffness as proposed by Harnau *et al.* [22] is the focus of future work.

H. Morhenn and T. Unruh gratefully acknowledge computation time granted by the Leibniz-Rechenzentrum der Bayerischen Akademie der Wissenschaften and financial support by the DFG (Grant No. UN267/4-1).

*hmorhenn@frm2.tum.de
†tobias.unruh@fau.de

[1] P. E. Rouse, J. Chem. Phys. **21**, 1272 (1953).
[2] J. Han, R. L. Jaffe, and D. Y. Yoon, Macromolecules **30**, 7245 (1997).
[3] W. Paul, G. D. Smith, D. Y. Yoon, B. Farago, S. Rathgeber, A. Zirkel, L. Willner, and D. Richter, Phys. Rev. Lett. **80**, 2346 (1998).
[4] K. Karatasos and D. B. Adolf, J. Chem. Phys. **112**, 8225 (2000).
[5] K. Karatasos and J.-P. Ryckaert, Macromolecules **34**, 7232 (2001); D. M. Whitley and D. B. Adolf, Mol. Simul. **38**, 119 (2012).
[6] S. D. Hotston, D. B. Adolf, and K. Karatasos, J. Chem. Phys. **115**, 2359 (2001).
[7] J. Farago, H. Meyer, and A. N. Semenov, Phys. Rev. Lett. **107**, 178301 (2011); J. Farago, H. Meyer, J. Baschnagel, and A. N. Semenov, J. Phys. Condens. Matter **24**, 284105 (2012).
[8] T. Unruh, J. Neuhaus, and W. Petry, Nucl. Instrum. Methods Phys. Res., Sect. A **580**, 1414 (2007); **585**, 201 (2008).
[9] H. Morhenn, S. Busch, and T. Unruh, J. Phys. Condens. Matter **24**, 375108 (2012).
[10] P. J. Flory and A. Vrij, J. Am. Chem. Soc. **85**, 3548 (1963).
[11] J. Wuttke, Physica B: Condensed Matter **266**, 112 (1999).
[12] B. Hess, C. Kutzner, D. V. D. Spoel, and E. Lindahl, J. Chem. Theory Comput. **4**, 435 (2008).
[13] J. Chang and S. I. Sandler, J. Chem. Phys. **121**, 7474 (2004).
[14] S. W. I. Siu, K. Pluhackova, and R. A. Böckmann, J. Chem. Theory Comput. **8**, 1459 (2012).
[15] T. Róg, K. Murzyn, K. Hinsen, and G. R. Kneller, J. Comput. Chem. **24**, 657 (2003).
[16] D. S. Pearson, G. V. Strate, E. von Meerwall, and F. C. Schilling, Macromolecules **20**, 1133 (1987); D. S. Pearson, L. J. Fetters, W. W. Greassley, G. V. Strate, and E. von Meerwall, Macromolecules **27**, 711 (1994).
[17] M. Doi and S. F. Edwards, *The Theory of Polymer Dynamics* (Oxford University Press, Oxford, 1986); D. Richter, M. Monkenbusch, A. Arbe, and J. Colmenero, Adv. Polym. Sci. **174**, 1 (2005).
[18] J. Farago, A. N. Semenov, H. Meyer, J. P. Wittmer, A. Johner, and J. Baschnagel, Phys. Rev. E **85**, 051806 (2012).
[19] J. Farago, H. Meyer, J. Baschnagel, and A. N. Semenov, Phys. Rev. E **85**, 051807 (2012).
[20] W. Paul, G. D. Smith, and D. Y. Yoon, Macromolecules **30**, 7772 (1997).
[21] S. W. Provencher, Comput. Phys. Commun. **27**, 213 (1982).
[22] L. Harnau, R. G. Winkler, and P. Reineker, J. Chem. Phys. **106**, 2469 (1997).